Aalborg Universitet

Multi-time Scale Fault Characteristics of HVDC-Connected Offshore Wind Farm and the Coordination with Different Protection Schemes

A Review

Gao, Guoqing; Blaabjerg, Frede; Wang, Yanbo

Multi-time Scale Fault Characteristics of HVDC-Connected Offshore Wind Farm and the Coordination with Different Protection Schemes: A Review

Guoqing Gao, Frede Blaabjerg, Yanbo Wang
AAU Energy, Aalborg University, Aalborg, Denmark
gga@energy.aau.dk, fbl@energy.aau.dk, ywa@energy.aau.dk

Keywords

« Protection device », « Modular Multilevel Converters (MMC)», « Wind energy ».

Abstract

The high-voltage dc (HVDC)-connected offshore wind farm is a power electronic converter dominated power system. Yet, the highly controlled fault characteristics of converters could affect the efficacy of different protection schemes. This paper first gives an overview of the multi-time scale fault characteristics of converters and the related different protection schemes. Then, the coordinated fast-time scale fault control of converters with the corresponding protection relays is summarized. Lastly, the protection schemes in slow-time scale are investigated, then the modified settings and criteria for these protection schemes are proposed considering the converter fault dynamics.

1. Introduction

With the substantial unexploited wind resources and the ideal wind conditions, offshore wind farms (OWFs) are increasingly being built worldwide for the large-scale use of renewable energy [1]. The modular multilevel converter (MMC) based high-voltage dc (HVDC) transmission system is a preferred solution for large OWFs for its flexible control capability [2]. The HVDC connected OWF is a converter-dominated power system with highly controlled multi-time scale fault behaviors. The highly controlled fault characteristics could lead to the malfunctions of different protection relays, which are typically designed and adjusted based on the characteristics of synchronous generators (SGs) [3].

The transient dynamics of the conventional SG-dominated system after fault inception involves mainly the sub-transient, transient, and synchronous dynamics. They can be characterized by the varying reactance behind an ideal voltage source. The sub-transient reactance can be in the range of 0.09 - 0.17 p.u. resulting in an inductive fault current with the peak ac-component of over six times rated [4]. The sub-transient and transient dynamics could last for several fundamental power cycles, which are coordinated with the most protection relays, e.g., the current differential protection (CDP), distance protection (DP), and overcurrent protection (OCP) [5]. In addition, SGs exhibit the swing characteristic due to the physical rotating mass with the inherent inertia and damping [6]. The swing characteristics of SGs are widely utilized to coordinate with the power swing blocking (PSB) [7] and out-of-step-tripping (OST) [8] to block the protection relays during a stable power swing and initiate the system partitioning in the event of an unstable swing.

The grid-side converters of the offshore wind turbines mainly adopt the grid-following (GFL) control, which is composed of the slow-time scale phase-locked loop (PLL) for synchronization and the fast-time scale vector current control for power injection [3]. In addition, the grid-side converters of the offshore wind turbines could adopt the grid-forming (GFM) control to support the grid voltage during contingency [9] or to form the grid voltage in diode rectifier unit (DRU) based HVDC system [10]. The common structure of the GFM control consists of different function layers to emulate the electromechanical and electromagnetic dynamics of SGs [11]. The offshore MMC station typically adopts the GFM control with the constant voltage/frequency (VF) control structure to operate as an ideal voltage source to form the offshore ac grid [12]. In addition, the power synchronization control (PSC) based GFM control is an alternative for the offshore MMC station [13]. Neither the VF-GFM control nor the PSC-GFM control has the inertia control characteristics.

The transient dynamics of power converters after fault inception can be mainly classified as the fast-time scale electromagnetic dynamics and the slow-time scale electromechanical dynamics. The electromagnetic dynamics mainly include the initial current spikes and the fast current-loop
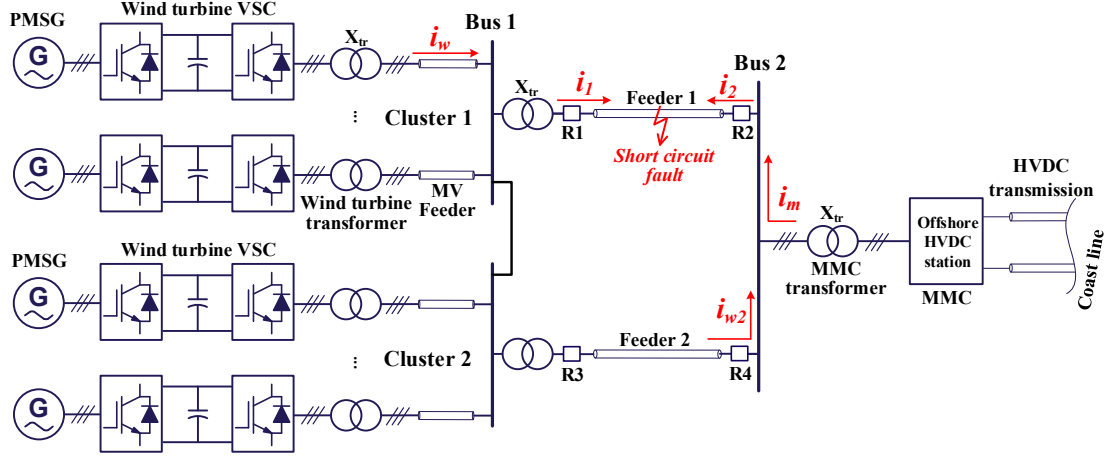
Fig. 1: Single-line diagram of the HVDC-connected offshore wind farm with a short-circuit fault in Feeder 1.

dynamics. The slow-time scale electromechanical dynamics mainly include the current-angle swing of the GFM converter and the voltage-angle swing of the GFL converter [14]. The multi-time scale fault characteristics of converters could have significant effect on the efficacy of different protection relays [15]. Considering the fast-time scale fault current control dynamics, a coordinated fault current phase angle control of converters with the DP is proposed in [16] for wind farms directly connected to the main ac grid. The influence of both the controlled fault current and the wind farm fault capacity on the CDP is investigated in [17]. In addition, the flexible converter control and the reduced inertia could significantly affect the slow-time scale dynamics of the system, thereby leading to the failure of the PSB and OST especially with the increasing proportion of the wind farm penetration. Thus, the optimized relay settings are proposed in [18] to cope with the PSB and OST failure.

However, the above-mentioned methods are only applicable to wind farms directly connected to the main ac grid. As for the offshore MMC station interfaced wind farm, both sides are power converters with highly controlled fault currents. The effect of the flexibly controlled fault current of the MMC on the efficacy of the DP, CDP, and OCP is investigated in [19]. Accordingly, a coordinated fault current control of the MMC is proposed in [20] to improve the efficacy of the CDP by aligning the fault currents on both sides. In addition, a soft current limiter is proposed in [21] to limit the fault current and generate the interharmonic current, which can be identified by a specially designed interharmonic differential relay to detect the faults in the inverter-based islanded microgrids. The interharmonic

differential relay has also the potential to be applied to the offshore MMC formed offshore ac grid. As for the slow-time scale PSB and OST, the optimized relay settings [18] for wind farms directly connected to the main ac grid is not suitable for the MMC-OWF system with completely controlled transient dynamics. To solve this problem, new criteria for the PSB and OST in the MMC-OWF system should be proposed considering the slow-time scale dynamics of the power converters.

The rest of the paper is organized as follows. The system description and the multi-time scale characteristics of converters are elaborated in Section 2. The coordinated converter control with the CDP, DP, and OCP is proposed in Section 3 by exploiting the fast-time scale characteristics. In addition, the new criteria for the PSB and OST are proposed in Section 4 by exploiting the slow-time scale characteristics. The new criteria are then validated using electromagnetic transient (EMT) simulations.

2. Multi-time scale characteristics of converters

A system diagram of the HVDC-connected OWF is illustrated in Fig. 1. The grid side voltage source converter (VSC) of wind turbines adopts the GFL control to inject the required active and reactive currents. After fault inception, the injected active and reactive currents of the GFL-VSC should follow the grid codes [22], which means that the phase angle φ_w of the fault current i_w from the GFL-VSC is determined. The PLL of the GFL-VSC tracks the phase angle θ_{PLL} of the voltage at the point of common coupling (PCC), which is subsequently utilized in the current control loop as
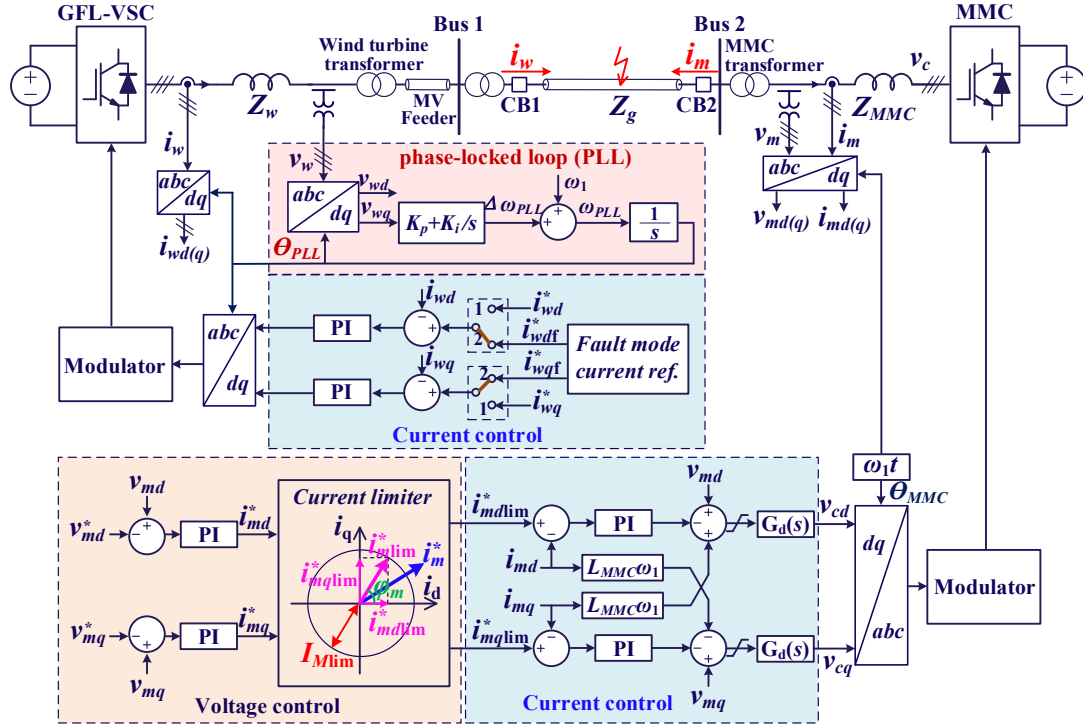
Fig. 2: Simplified controller block diagram of the HVDC-connected offshore wind farm.
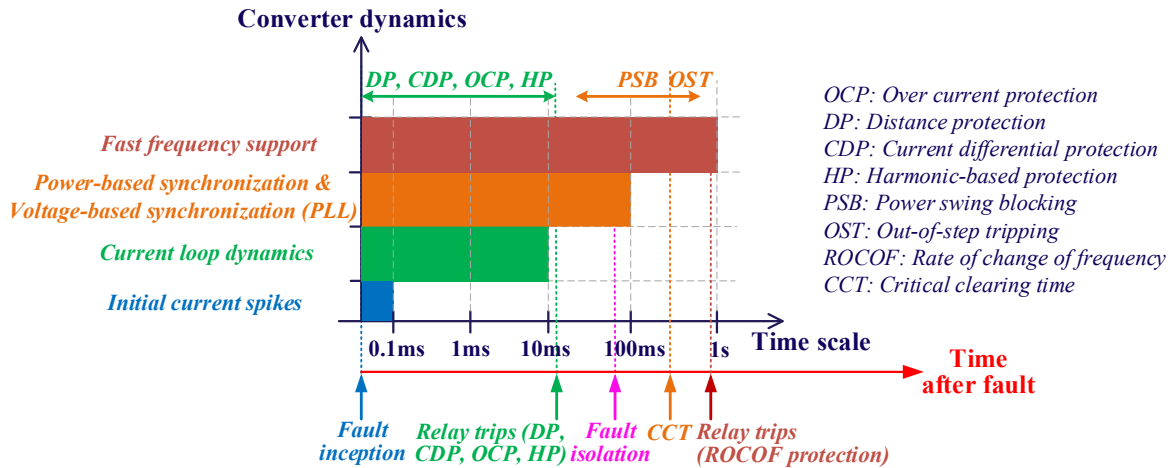

Fig. 3: Multi-time scale characteristics of converters and the coordination with different protection schemes in a HVDC connected wind farm.

shown in Fig. 2. The offshore MMC station adopts the GFM control to regulate the voltage and frequency of the offshore ac grid [19]. After a low-impedance short circuit fault, the terminal voltage v_m of the MMC cannot be controlled and the current limiter is in an active mode to limit the magnitude of the fault current i_m from the MMC. However, the phase angle of the limited fault current i_m can be controlled with a high flexibility to an arbitrary value.

After the inception of a short-circuit fault, the converter dynamics involve mainly the initial transient current spikes, current loop dynamics, synchronization dynamics, and the fast frequency support. Their interactions with the harmonic-based protection (HP), CDP, DP, OCP, PSB, OST, and the rate of change of frequency (ROCOF) protection are illustrated in Fig. 3. The initial current spikes are related to the filter capacitor, pre-fault condition, fault angle, system impedance, etc., at the time scale around hundreds of microseconds (e.g., 100 us) [4]. Thus, the initial current spikes do not have significant impact on the efficacy of the above-mentioned protections, whereas the current loop dynamics, synchronization dynamics, and the fast frequency support could affect the efficacy of the protection relays.

2.1 Fast current loop dynamics

The rise time of the current loop is in the time scale of several milliseconds (e.g., 2 ms), which is within the operating time of the OCP, DP, and CDP. The fast current control dynamics are the premise of the coordinated fault current control of converters with the protection relays by injecting an optimized fault-ride-through (FRT) current, which is conductive to the fast relay tripping of the OCP, DP, and CDP [19]. In addition, the fast current control of converters can be coordinated with the specially designed HP by injecting the inter-harmonic current [21] or the synthetic harmonic current [23] during a short-circuit fault.

2.2 Slow-time scale dynamics

2.2.1 Synchronization dynamics

The synchronization methods of grid-connected converters can mainly be classified as the power-based synchronization and the voltage-based synchronization [24]. The power-based synchronization can be realized by different control methods, such as the droop control, power synchronization control (PSC), virtual synchronous (VSG) control, synchronverter, etc. The different control methods differ in terms of inertia support, transient stability, operation characteristics, etc. The power-based synchronization control is in the time-scale around 100 ms [25]. Besides, the voltage-based synchronization is typically realized by the PLL. The settling time of the PLL is in the time scale of tens of milliseconds (e.g., 40 ms) [26].

After the inception of a short-circuit fault at the offshore ac grid of the MMC station connected offshore wind farm as shown in Fig. 1, the impedance trajectory and the rate of change of the impedance measured by a distance relay are highly affected by the PLL dynamics, which is different from the SG-dominated system. Since the PSB is used to differentiate between a fault and power swing according to the measured impedance [27], parameter settings of the PSB should be adjusted according to the PLL dynamics to block the operation of distance relays in the event of a power swing. Otherwise, the distance relays could mistake the power swing as a fault condition and trip the circuit breakers.

The critical clearing time (CCT) of a short-circuit fault in the MMC station connected offshore wind farm is also affected by the PLL dynamics. If there is a short-circuit fault on Feeder 1 as shown in Fig.

1, the DP will trip the circuit breakers controlled by the relay R1 and R2 to isolate the fault within a short time. After fault inception, the generated power from Cluster 1 should be transferred to the offshore MMC station through Feeder 2 to reach a new state of equilibrium, which is affected by the PLL dynamics. However, if the short-circuit fault cannot be isolated before the CCT due to a stuck breaker, the system could become out-of-step (unstable power swing) and the OST will initiate the system partitioning to avoid equipment damage and a widespread power outage. If the fault is isolated before the CCT, the system will become stable and the OST will not be initiated.

2.2.2 Fast frequency support

With the increasing wind farm integration, the power system inertia level continues to decrease. Since the ROCOF is inversely proportional to the system inertia, a disturbance such as power imbalance could lead to a significant ROCOF in the system integrated with HVDC-connected offshore wind farms. Thus, the revised grid codes of National Grid UK increase the ROCOF from 0.125 Hz/s to 1 Hz/s to avoid the malfunction of ROCOF relays due to the decreasing system inertia [28]. If the measured ROCOF breaches a predefined value, a ROCOF relay could mistakenly interpret the high ROCOF as loss of main (LOM) and subsequently disconnect the wind farms [15]. To avoid the malfunction of the ROCOF protection, the fast frequency support from wind turbine converters and the offshore MMC station is proposed to support the onshore grid frequency during a frequency dip [29].

3. Coordination of Fast-Scale Dynamics with CDP, DP and OCP

Since the fast current loop dynamics of converters is within the operating time of the DP, CDP, and OCP, the fault current control of converters can be coordinated with these protection schemes. In addition, the DP, CDP, and OCP are designed based on the fault characteristics of the SG-dominated power system where the fault current phase angles of both sides of the protected line are similar. Thus, the coordinated fault current control of the converters can be proposed by emulating this characteristic.

3.1 Current differential protection (CDP)

A coordinated fault current control of the MMC with the CDP is proposed in [20] and the corresponding basic idea is illustrated in Fig. 4.

(a) Randomly controlled fault current of the MMC.

(b) Coordinated fault current control of the MMC.

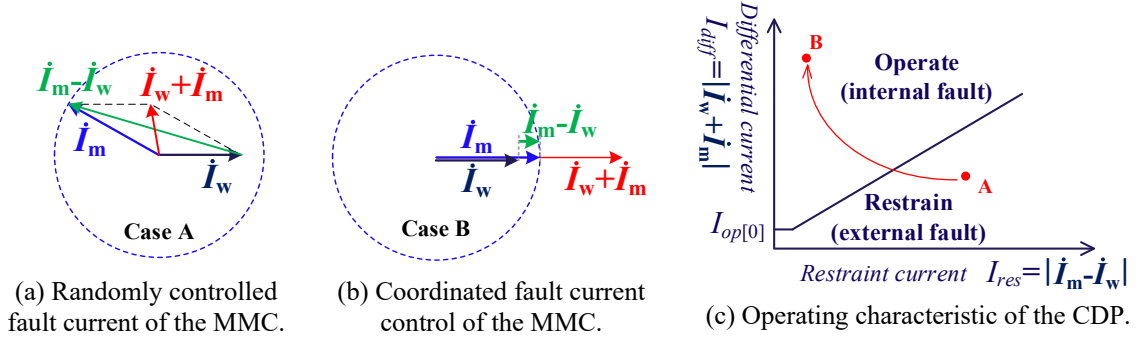(c) Operating characteristic of the CDP.

Fig. 4: Coordinated control of the MMC with the current differential protection (CDP).
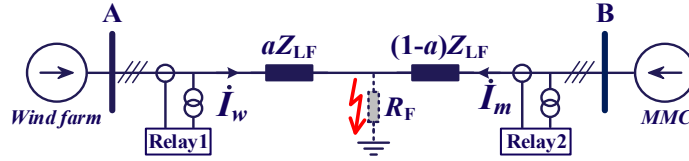

Fig. 5: Simplified system diagram of the MMC connected offshore wind farm with distance protection relays on both sides of the protected feeder.
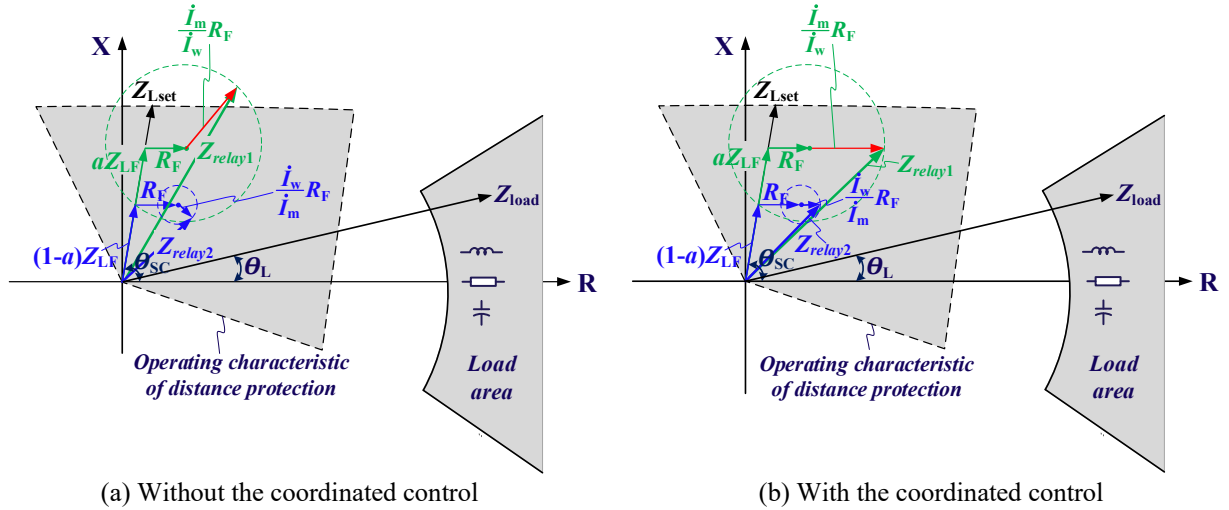

(a) Without the coordinated control

(b) With the coordinated control

Fig. 6: The measured impedances by Relay 1 and Relay 2 after fault inception.

The fault current vector $\dot{I}_w$ from wind turbine VSCs should follow the grid codes [22] with the determined phase angle, while the phase angle of the fault current $\dot{I}_m$ from the MMC can be controlled with a high flexibility. If the phase difference between $\dot{I}_m$ and $\dot{I}_w$ is much greater than 90° (case A), the CDP relay fails to trip corresponding to point A of Fig. 4. However, if $\dot{I}_m$ is controlled to be aligned with $\dot{I}_w$ according to the coordination method, the relay can successfully trip corresponding to point B.

3.2 Distance protection (DP)

A simplified system diagram of the MMC connected offshore wind farm during a short-circuit fault with the fault resistance R_F is

illustrated in Fig. 5. Z_{LF} represents the feeder impedance. The parameter a $(0 \leq a \leq 1)$ is determined by the fault location. As expressed in (1), the measured impedances by Relay 1 and Relay 2 (i.e., Z_{relay1} and Z_{relay2}) are the sum of three vectors, respectively.

$$
\begin{aligned}
Z_{\text{relay1}} &= aZ_{LF} + R_F + \frac{\dot{I}_m}{\dot{I}_w} R_F \\
Z_{\text{relay2}} &= \left(1-a\right)Z_{LF} + R_F + \frac{\dot{I}_w}{\dot{I}_m} R_F
\end{aligned}
\tag{1}
$$

The coordinated fault current control of the MMC with the CDP is also conducive to the successful tripping of the DP as explained in Fig. 6. If the coordinated fault control of the MMC is not
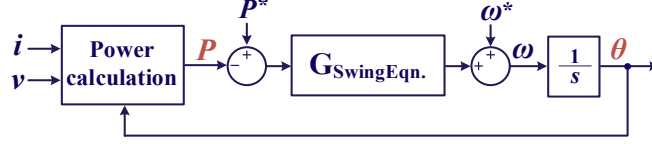
Fig. 7: Simplified *P-θ* swing characteristics of the SGs or GFM converters.
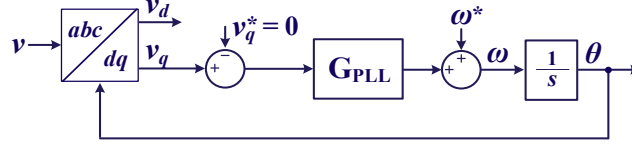

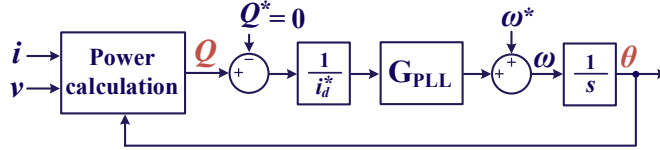Fig. 8: Block diagram of the PLL used in wind turbines.

Fig. 9: *Q-θ* swing characteristics of the GFL converters.

applied, the phase angle of the vector $(\dot{I}_m / \dot{I}_w)R_F$ can be an arbitrary value, which could lead to the failure of the DP when Z_{relay1} crosses the operating characteristic as shown in Fig. 6(a). When the coordinated control of the MMC is applied to align $\dot{I}_m$ with $\dot{I}_w$, Z_{relay1} will get inside of the operating characteristic to ensure the successful tripping of the DP after fault inception like shown in Fig. 6(b).

3.3 Overcurrent protection (OCP)

After a short-circuit fault on Feeder 1 as illustrated in Fig. 1, the fault current i_2 flowing through the OCP relay R2 is the sum of the fault current i_m from the MMC and the fault current i_{w2} from wind farm Cluster 2. When the coordinated fault current control of the MMC is applied, the magnitude of i_2 is the maximum value since i_m is aligned with i_{w2}. Otherwise, i_m and i_{w2} could cancel out each other leading to a reduced magnitude of i_2 [30]. Therefore, the coordinated fault control of the MMC can increase the magnitude of i_2, thereby increasing the speed of the overcurrent relay R2 since the operating time of the overcurrent relay is negatively correlated with the magnitude of the fault current flowing through it [19].

4. Coordination of slow-scale dynamics with PSB and OST

4.1 Power swing

Power swing of the conventional SG-based power system refers to the variation of power flow when

the generator rotor angles advance or retard relative to each other consequent to a large disturbance such as system faults and the line switching [31]. The *P-θ* swing characteristics of the conventional power system [6] can be simplified as shown in Fig. 7. To mimic the electromechanical characteristics of SGs, the GFM converters could implement the swing equation of SGs with the virtual inertia and damping [32], [33]. Thus, the *P-θ* swing characteristics of SGs as illustrated in Fig. 7 is also applicable to some GFM converters. For instance, the power swing dynamics of the virtual synchronous generator (VSG), a type of GFM converter, can be characterized by the swing equation with the bandwidth of a few Hertz [11].

The grid side converters of wind turbines generally adopt the GFL control. During normal operation, the injected active and reactive currents are expressed in (2). Besides, a PLL is required for the GFL converter to get synchronized with the grid voltage. A block diagram of the PLL is shown in Fig. 8. During the steady state, v_q is equal to zero since the GFL converter is synchronized with the grid voltage. Therefore, the injected reactive power Q is equal to zero according to (3). During the transient state, the injected reactive power Q is equal to $v_q i_d^*$. Accordingly, the *Q-θ* swing characteristics of the GFL converter [14] is illustrated in Fig. 9. The generalized swing equation of the GFL converter with the equivalent inertia and damping is derived in [34] to analyze the electromechanical dynamics. Besides, a
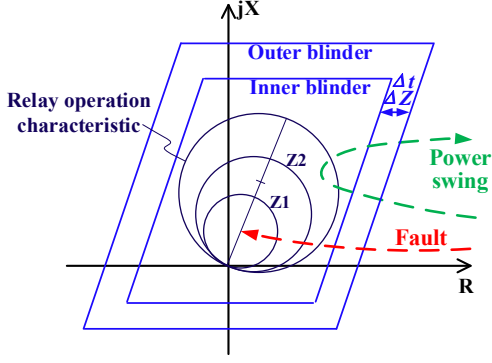
Fig. 10: Illustration of the PSB blinders and the impedance trajectories during a short-circuit fault and a power swing.

modified PLL is proposed in [35], which can achieve an enhanced inertia and damping emulation to provide the fast frequency support.

$$i_d = i_d^*$$
$$i_q = i_q^* = 0 \tag{2}$$

$$Q = v_q i_d - v_d i_q = \begin{cases} 0 & \textit{Steady state} \\ v_q i_d^* & \textit{Transient state} \end{cases} \tag{3}$$

4.2 Power swing blocking (PSB)

A power swing could cause the measured impedance trajectory to enter the operating characteristic of a distance relay and subsequently the false tripping of the relay. The short circuit fault is an electromagnetic transient process with a time constant of a few milliseconds, whereas the power swing of the conventional SG-based power system is an electromechanical transient process with a much longer time constant of a few seconds [36]. Therefore, the PSB is utilized to distinguish between the short circuit fault and power swing based on their different transient dynamics, then block the operation of the target distance relay in the event of a power swing [18].

The impedance measured by a distance relay immediately jumps from the load impedance to the fault impedance inside the relay operation characteristic after a short-circuit fault. On contrary, the impedance trajectory of a power swing exhibits the steady progression and may move inside the relay operation characteristic as illustrated in Fig. 10. Therefore, the PSB of the MMC-OWF system can be implemented involving three steps:

1. Calculate the maximum rate of change of impedance ($\Delta Z/\Delta T$) during the power swing. The rate of change of impedance in a conventional SG-dominated system is determined by the system inertia. Due to the reduced inertia and the fast converter control in the MMC connected offshore wind farm, the maximum rate of change of impedance is significantly increased and it is determined by the converter dynamics.

2. Choose the outer and inner blinders surrounding the relay operation characteristic with the distance of ΔZ, then count the time Δt it takes for impedance trajectory to cross the blinders.

3. If the calculated rate of change of impedance $\Delta Z/\Delta t$ is less than the maximum rate $\Delta Z/\Delta T$ for the power swing, a power swing is declared and the PSB is initiated to avoid an undesired relay tripping when the measured impedance trajectory enters the relay operation characteristic.

The EMT simulation of a bolted symmetrical three-phase-to-ground fault on Feeder 1 for 500 ms as illustrated in Fig. 1 is conducted to investigate the characteristics of impedance trajectories measured by relays at different locations. The main system parameters used in this simulation are shown in Table I. The fault current response of the converters on both sides are elaborated in Section 2. Since the fault location is within the protected range of relay R1, the measured impedance by R1 immediately jumps into the relay operation characteristic after fault inception as shown in Fig. 11(a). The rate of change of the measured impedance is very fast after fault inception, which is determined by the time-constant of the signal filtering mechanism of the relay [15]. Conversely, the fault location on Feeder 1 is beyond the protected range of relay R3. The measured impedance by R3 is the swing impedance, the rate of change of which is slow and determined by the PLL dynamics as shown in Fig. 11(b). Although the measured swing impedance by relay R3 enters its operation characteristic, the trip of R3 is blocked by the PSB since the rate of change of Z_{R3} is less than the maximum rate of a power swing.

4.3 Out-of-step tripping (OST)

The power swing can be classified as a stable power swing and an unstable power swing (out-of-step). The system can regain a new state of equilibrium after the stable power swing. On contrary, the system will experience the loss of synchronization (LOS) with an unstable power swing. The asynchronous power system areas must be separated from each other quickly to
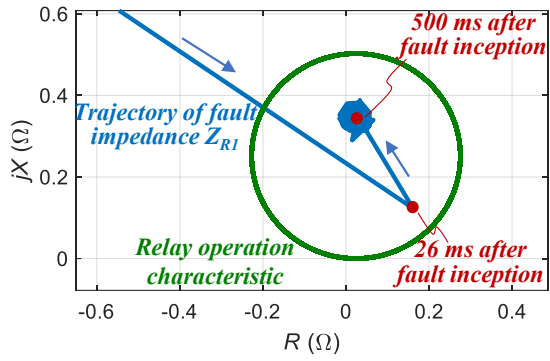
(a) Measured impedance by relay R1
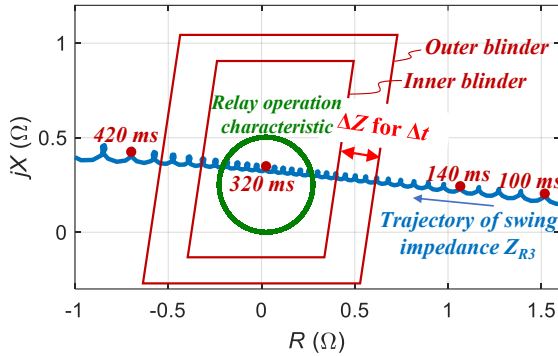
(b) Measured impedance by relay R3

Fig. 11: Measured impedance by different relays at different locations after fault inception.

Table I: MAIN SYSTEM PARAMETERS USED IN SIMULATIONS

Symbol	Meaning	Values
P	Power rating of the offshore wind farm	100 MW
V_m	RMS value of the rated ac voltage of MMC	210 kV
f_l	Nominal grid frequency	50 Hz
V_w	RMS value of the rated ac voltage of wind turbine VSC	0.69 kV
I_{lim}	Limit value of the current from converters	1.2 p.u.
X_{tr}	Leakage reactance of transformers	0.12 p.u.

avoid equipment damage and a widespread power outage. Therefore, the OST is applied to differentiate between a stable and unstable swing as illustrated in Fig. 12 and initiate the system partitioning in the event of an unstable swing. The implementation of the OST for the conventional SG-dominated system is based on the following criteria [37]:
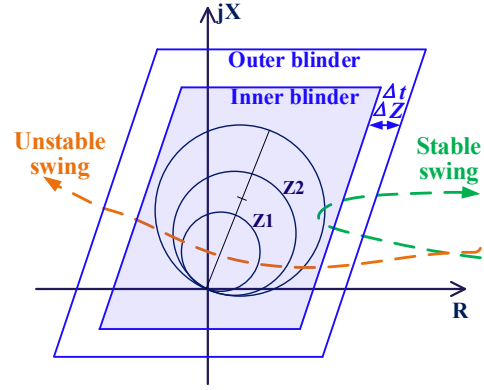

Fig. 12: Characteristics of the measured impedance trajectories of the stable and unstable swing in SG-dominated system.

1. The OST function declares an unstable swing as soon as the measured impedance trajectory passes through the area surrounded by the inner blinder.

2. If the sign of the R components of the impedance are the same when the measured trajectory enters and exits the inner blinder, a stable swing is declared.

With the large-scale integration of wind farms to the conventional SG-based power system, the LOS due to grid faults or large system disturbances should be addressed by the OST, which involves the tripping of some wind farms [38], [39]. However, the above-mentioned criteria for the OST are based on the mathematical model where the interconnected systems are completely formed with SGs [36]. Thus, the OST could malfunction with the wind farm penetration. To solve this problem, the modified settings for the OST is proposed in [18]. In addition, the offshore ac grid of the MMC-OWF system is completely interfaced with converters and there is no SG connected. The characteristics of the stable and unstable swing impedance trajectories of the MMC-OWF system are different from the conventional SG-based system or the SG-based system with wind farm penetration. Thus, the conventional OST could fail in the MMC-OWF system due to the different converter dynamics.

Simulation results of a stable power swing after a bolted symmetrical three-phase-to-ground fault on Feeder 1 for 500 ms are illustrated in Fig. 13. Since the converter dynamics and the impedance trajectories are determined by the converter control, the measured impedance Z_{R3} by relay R3 is highly controlled. Although the trajectory of the swing impedance passes through the inner blinder
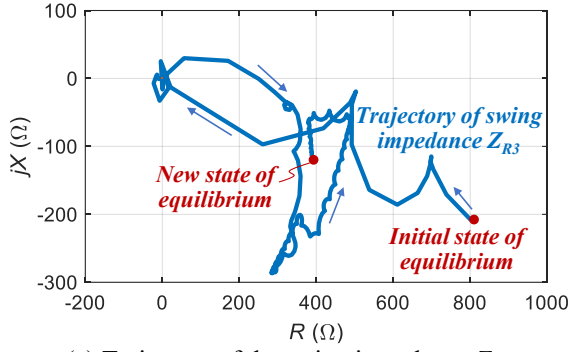
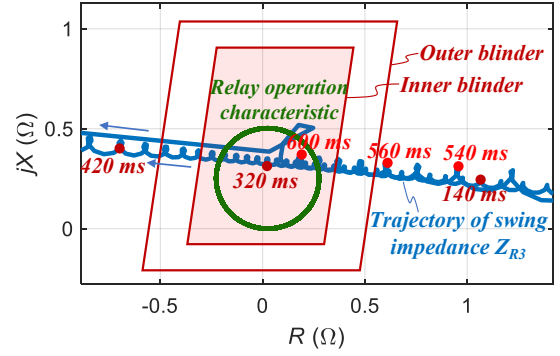(a) Trajectory of the swing impedance Z_{R3}
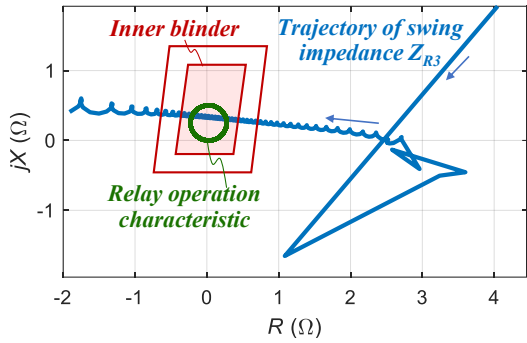
(b) Zoom-in trajectory of Z_{R3}
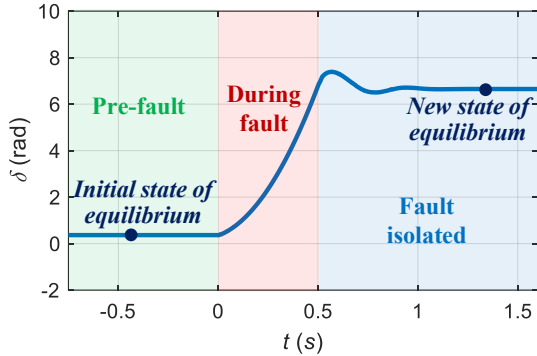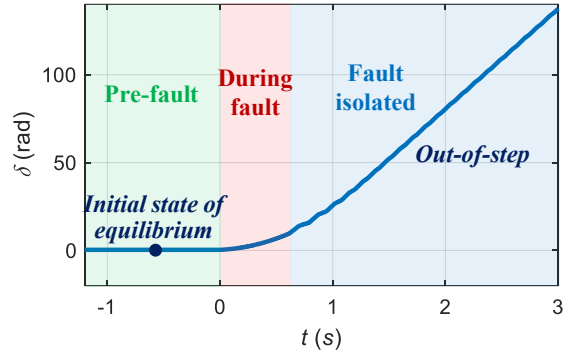

(c) Waveform of the power angle δ

Fig. 13: Stable power swing after a bolted symmetrical three-phase-to-ground fault for 500 ms.

as shown in Fig. 13(b), it is essentially a stable power swing since the system reaches a new state of equilibrium. The measured impedance at this new equilibrium corresponds to the new load impedance. The waveform of the power angle δ also validates that the system is undergoing a stable power swing, which gradually converges to a new equilibrium point. However, the conventional OST will lead to an undesired system partitioning in this case by mistakenly declaring an unstable power swing when the measured impedance trajectory passes through the inner blinder.

To avoid the malfunction of the conventional OST, a new criterion for the OST of the MMC-OWF system should be proposed. The stable

(a) Trajectory of the swing impedance Z_{R3}

(b) Waveform of the power angle δ

Fig. 14: Unstable power swing (out-of-step) after a bolted symmetrical three-phase-to-ground fault on Feeder 1 for 600 ms.

power swing regains a new state of equilibrium after the disturbances. Accordingly, the measured impedance trajectory only passes through the inner blinder once for the MMC-OWF system. On contrary, the power angle during an unstable power swing continuously increases instead of reaching the state of equilibrium. The trajectory of the swing impedance in this case will pass through the inner blinder multiple times. Therefore, a new criterion for the OST of the MMC-OWF system can be selected as: the trajectory of swing impedance passes through the inner blinder twice.

Simulation results of an unstable power swing (out-of-step) after a bolted symmetrical three-phase-to-ground fault on Feeder 1 for 600 ms are illustrated in Fig. 14. Since the fault is not cleared within the critical clearing time (CCT), the system will experience an out-of-step. The power angle δ continuously increases after fault inception, which indicates an unstable power swing of the system. As a result, the trajectory of the unstable swing impedance Z_{R3} crosses the inner blinder multiple times after fault inception. According to the proposed new criterion, OST is initiated to partition the unstable MMC-OWF system to avoid equipment damage and a widespread power outage.

5. Conclusion

This paper has given a review of the multi-time scale fault characteristics of converters and the corresponding protection schemes in the offshore ac grid that interfaces the grid-side converters of wind turbines and the offshore MMC station. In the fast-time scale, a coordinated fault control of the MMC with the CDP, DP, and OCP is presented by exploiting the fault characteristics of wind turbine converters and the operation characteristics of relays. In the slow-time scale, the effect of power swing dynamics on the PSB and OST due to the synchronization process of converters are investigated. Accordingly, the modified criteria and settings for the PSB and OST in the OWF-MMC system are proposed and subsequently validated by the EMT simulations.

References

[1] F. Blaabjerg, Y. Yang, K. A. Kim and J. Rodriguez, "Power Electronics Technology for Large-Scale Renewable Energy Generation," in *Proc. IEEE*, vol. 111, no. 4, pp. 335-355, April 2023, doi: 10.1109/JPROC.2023.3253165.

[2] U. Karaagac, J. Mahseredjian, L. Cai, and H. Saad, "Offshore wind farm modeling accuracy and efficiency in MMC-based multiterminal HVDC connection," *IEEE Trans. Power Del.*, vol. 32, no. 2, pp. 617–627, Apr. 2017.

[3] H. Zhang, W. Xiang, W. Lin, and J. Wen, "Grid forming converters in renewable energy sources dominated power grid: Control strategy, stability, application, and challenges," *J. Mod. Power Syst. Clean Energy*, vol. 9, no. 6, pp. 1239–1256, Nov. 2021.

[4] N. C. Ekneligoda, R. G. Ramakumar, P. Moses, J. Jiang, D. Wu, K. Smedley, and K. Prabakar, "An overview of issues relevant to protection and restoration of PV systems at distribution level," *in 2021 IEEE PES General Meeting*, Denver, Colorado, USA, July 25-29, 2021, pp. 1-5.

[5] S. Manson, and E. McCullough, "Practical Microgrid Protection Solutions: Promises and Challenges," *in IEEE Power and Energy Magazine*, May-June 2021, vol. 19, no. 3, pp. 58-69, doi: 10.1109/MPE.2021.3057953.

[6] J. D. Glover and M. S. Sarma, *Power System Analysis and Design*, 3rd ed. Boston, MA: PWS, 2001.

[7] L. Martuscello, E. Krizauskas, J. Holbach, and Y. Lu, "Tests of distance relay performance on stable and unstable power swings reported using simulated data of the August 14th 2003 system disturbance," *in Proc. IEEE 62nd Annu. Conf. Protect. Relay Eng.*, May 2009, pp. 236–255.

[8] F. Gonzalez-Longatt, C. Adiyabazar, and E. V. Martinez, "Setting and Testing of the Out-of-Step Protection at Mongolian Transmission System," *Energies*, vol. 14, no. 23, pp. 8170-8205, Dec. 2021, doi: 10.3390/en14238170.

[9] T. Neumann et al., "Noval direct voltage control by wind turbines," in *Proc. IEEE Power Energy Soc. General Meeting*, Boston, MA, USA, Jul. 2016, pp. 1–5.

[10] S. Seman, R. Zurowski, and C. Taratoris, "Interconnection of advanced type 4 WTGs with diode rectifier based HVDC solution and weak AC grids," *in Proc. 14th Wind Integr. Workshop*, Brussels, Belgium, Oct. 2015, pp. 1–7.

[11] G. Wang, L. Fu, Q. Hu, C. Liu, and Y. Ma, "Small-signal synchronization stability of grid-forming converter influenced by multi time-scale control interaction," *Energy Reports*, vol. 9, pp. 597-606, 2023.

[12] K. Schönleber, E. Prieto-Araujo, S. Ratés-Palau, and O. Gomis-Bellmunt, "Handling of unbalanced faults in HVDC-connected wind power plants," *Electric Power Systems Research,* vol. 152, pp. 148-159, 2017.

[13] P. Mitra, L. Zhang, and L. Harnefors, "Offshore Wind Integration to a Weak Grid by VSC-HVDC Links Using Power-Synchronization Control: A Case Study," *IEEE Trans. Power Del.,* vol. 29, pp. 453-461, 2014.

[14] Y. Li, Y. Gu, and T. C. Green, "Revisiting Grid-Forming and Grid-Following Inverters: A Duality Theory," *IEEE Trans. Power Syst*, vol. 37, pp. 4541-4554, Feb. 2022.

[15] A. Haddadi, E. Farantatos, I. Kocar, and U. Karaagac, "Impact of Inverter Based Resources on System Protection," *Energies*, vol. 14, no. 4, pp. 1050-1071, Feb. 2021, doi: 10.3390/en14041050.

[16] K. Ma, Z. Chen, Z. Liu, C. L. Bak, and M. Castillo, "Protection collaborative fault control for power electronic-based power plants during unbalanced grid faults," *Int. J. Elect. Power Energy Syst.*, vol. 130, pp. 107009–107016, Sep. 2021.

[17] Y. Li, K. Jia, T. Bi, R. Yan, W. Li, and B. Liu, "Analysis of line current differential protection considering inverter-interfaced renewable energy power plants," *in Proc. IEEE PES Innovat. Smart Grid Technol. Conf. Eur. (ISGT-Europe)*, Turin, Italy, Sep. 2017, pp. 1–6.

[18] A. Haddadi, I. Kocar, U. Karaagac, H. Gras, and E. Farantatos, "Impact of Wind Generation on

Power Swing Protection," *IEEE Trans. Power Del.*, vol. 34, pp. 1118-1128, Jan. 2019.

[19] G. Gao, H. Wu, and X. Wang, "Converter control impacts on efficacy of protection relays in HVDC-connected offshore wind farms," *in Proceedings of the 2022 IEEE 13th International Symposium on Power Electronics for Distributed Generation Systems (PEDG)*, Kiel, Germany, 26–29 June 2022; pp. 1–6.

[20] G. Gao, H. Wu, F. Blaabjerg, and X. Wang, "Fault current control of MMC in HVDC-connected offshore wind farm: A coordinated perspective with current differential protection," *Int. J. Elect. Power Energy Syst.*, vol. 148, p. 108952, Jun. 2023, doi: https://doi.org/10.1016/j.ijepes.2023.108952.

[21] W. T. El-Sayed, E. F. El-Saadany, and H. H. Zeineldin, "Interharmonic Differential Relay With a Soft Current Limiter for the Protection of Inverter-Based Islanded Microgrids," *IEEE Trans. Power Del.*, vol. 36, pp. 1349-1359, Jul. 2021.

[22] M. Graungaard Taul, X. Wang, P. Davari, and F. Blaabjerg, "Current reference generation based on next-generation grid code requirements of grid-tied converters during asymmetrical faults," *IEEE J. Emerg. Selected Topics Power Electron.*, vol. 8, no. 4, pp. 3784–3797, Dec. 2020.

[23] K. Saleh, M. A. Allam, and A. Mehrizi-Sani, "Protection of Inverter-Based Islanded Microgrids via Synthetic Harmonic Current Pattern Injection," *IEEE Trans. Power Del.*, vol. 36, pp. 2434-2445, May 2021.

[24] X. Wang, M. G. Taul, H. Wu, Y. Liao, F. Blaabjerg, and L. Harnefors, "Grid-synchronization stability of converter-based resources–an overview," *IEEE Open J. Ind. Appl.*, vol. 1, pp. 115–134, Aug. 2020.

[25] H. Sun, X. Lin, S. Chen, X. Ji, D. Liu, and K. Jiang, "Transient stability analysis of the standalone solar-storage AC supply system based on grid-forming and grid-following converters during sudden load variation," *IET Renew. Power Gener.*, vol. 17, pp. 1286-1302, Apr. 2022.

[26] R. Teodorescu, M. Liserre, and P. Rodriguez, *Grid Converters For Photovoltaic and Wind Power Systems*. Hoboken, NJ, USA: Wiley, 2011.

[27] G. Ziegler, *Numerical Distance Protection*. Hoboken, NJ, USA: Wiley, 2011.

[28] Q. Hong, M. A. U. Khan, C. Henderson, A. Egea-Àlvarez, D. Tzelepis, and C. Booth, "Addressing Frequency Control Challenges in Future Low-Inertia Power Systems: A Great Britain Perspective," *Engineering,* vol. 7, pp. 1057-1063, Aug. 2021.

[29] M. M. Kabsha and Z. H. Rather, "A new control scheme for fast frequency support from HVDC connected offshore wind farm in low inertia system," *IEEE Trans. Sustain. Energy*, vol. 11, no. 3, pp. 1829–1837, Jul. 2020.

[30] Y. Jing, R. Li, L. Xu, and Y. Wang, "Enhanced AC voltage and frequency control of offshore MMC station for wind farm connection," *IET Renew. Power Gener.*, vol. 12, no. 15, pp. 1771–1777, Sep. 2018.

[31] Y. G. Paithankar and S. R. Bhide, *Fundamentals of Power System Protection*. New Delhi, India: Prentice-Hall, 2010.

[32] M. Chen, D. Zhou, and F. Blaabjerg, "Modelling, implementation, and assessment of virtual synchronous generator in power systems," *J. Modern Power Syst. Clean Energy*, vol. 8, no. 3, pp. 399–411, May 2020.

[33] W. Zhang, A. M. Cantarellas, J. Rocabert, A. Luna, and P. Rodriguez, "Synchronous power controller with flexible droop characteristics for renewable power generation systems," *IEEE Trans. Sustain. Energy*, vol. 7, no. 4, pp. 1572–1582, Oct. 2016.

[34] R. Ma, J. Li, J. Kurths, S. Cheng, and M. Zhan, "Generalized Swing Equation and Transient Synchronous Stability With PLL-Based VSC," *IEEE Trans. Energy Convers.*, vol. 37, pp. 1428-1441, Dec. 2022.

[35] X. Guo, D. Zhu, J. Hu, X. Zou, Y. Kang, and J. M. Guerrero, "Inertial PLL of grid-connected converter for fast frequency support," *CSEE J. Power Energy Syst.*, early access, May 2022, doi: 10.17775/CSEEJPES.2021.08650.

[36] D. Tziouvaras and D. Hou, "Out-of-step protection fundamentals and advancements," *in Proc. 30th Annu. Western Protective Relay Conf.*, Spokane, WA, Oct. 21–23, 2003, pp. 282-307.

[37] Siemens AG, Energy Sector: User Manual Distance Protection 7SA522 V4.61, Ordering Nr. C53000-G1176-C155-5, [Online]. Available: http://www.siprotec.com

[38] O. Göksu, R. Teodorescu, C. L. Bak, F. Iov, and P. C. Kjær, "Instability of wind turbine converters during current injection to low voltage grid faults and PLL frequency based stability solution," *IEEE Trans. Power Syst.*, vol. 29, pp. 1683–1691, Jul. 2014.

[39] S. Ma, H. Geng, L. Liu, G. Yang, and B. C. Pal, "Grid-synchronization stability improvement of large scale wind farm during severe grid fault," *IEEE Trans. Power Syst.*, vol. 33, no. 1, pp. 216–226, Jan. 2018.